Development 140, 800-809 (2013) doi:10.1242/dev.089557

Par3/Bazooka and phosphoinositides regulate actin protrusion formation during *Drosophila* dorsal closure and wound healing

Karen Pickering[1,*], Juliana Alves-Silva[1,*], Deborah Goberdhan[2] and Tom H. Millard[1,‡]

SUMMARY

Effective wound closure mechanisms are essential for maintenance of epithelial structure and function. The repair of wounded epithelia is primarily driven by the cells bordering the wound, which become motile after wounding, forming dynamic actin protrusions along the wound edge. The molecular mechanisms that trigger wound edge cells to become motile following tissue damage are not well understood. Using wound healing and dorsal closure in *Drosophila*, we identify a direct molecular link between changes in cell-cell adhesion at epithelial edges and induction of actin protrusion formation. We find that the scaffolding protein Par3/Bazooka and the lipid phosphatase Pten are specifically lost from cell-cell junctions at epithelial edges. This results in a localized accumulation of phosphatidylinositol 3,4,5-trisphosphate (PIP3), which promotes the formation of actin protrusions along the epithelial edge. Depleting PIP3 results in defective epithelial closure during both dorsal closure and wound healing. These data reveal a novel mechanism that directly couples loss of epithelial integrity to activation of epithelial closure.

KEY WORDS: Wound, PIP3 [PtdIns(3,4,5)P_3], Filopodia, *Drosophila*

INTRODUCTION

An epithelium is a coherent sheet of cells that functions as a barrier, separating an organism or tissue from its environment. Any wounds that arise in an epithelium must be closed rapidly and completely to maintain barrier function. Closure of epithelial wounds is primarily driven by the cells bordering the wound, which undergo morphological changes following wounding, including the assembly of dynamic actin protrusions on the edge of the cell facing the wound (Martin, 1997). These planar-polarized protrusions promote wound closure by driving the movement of the epithelium across the wound, and also assist adhesion of the epithelial edges at the end of closure (Wood et al., 2002). Following wound closure, the wound edge cells revert to their normal epithelial morphology, re-establishing apicobasally polarized cell-cell junctions and disassembling actin protrusions (Garcia-Fernandez et al., 2009). Epithelial discontinuities similar to wounds also arise in the course of embryonic development and are closed in a similar manner (Martin and Parkhurst, 2004). For example, dorsal closure (DC) is a morphogenetic event that occurs during *Drosophila* embryogenesis, which has become a well-recognized model of epithelial closure (Harden, 2002). In particular, DC has proved a useful model for understanding the regulation and function of actin at epithelial edges (Kaltschmidt et al., 2002). Prior to DC, the dorsal surface of the embryo is covered by an extra-embryonic epithelium called the amnioserosa. During DC, the amnioserosa is displaced by the movement of the epidermis on the two sides of the embryo over the dorsal surface, until the epidermal edges meet and fuse (Harden, 2002). The cells at the dorsal edge of the advancing epidermis play a central role in driving DC. In these dorsal-most epidermal (DME) cells, the actin cytoskeleton becomes planar polarized, with a contractile actomyosin cable and dynamic filopodial actin protrusions forming at the leading edge of each cell (Jacinto et al., 2000; Kiehart et al., 2000). The actomyosin cable, which is connected from one cell to the next by adherens junctions, provides some of the force that drives closure of the dorsal hole, while the filopodia drive adhesion between the two epidermal edges, a process known as zippering (Jacinto et al., 2000; Kiehart et al., 2000; Millard and Martin, 2008). The parallels between DC and wound healing are particularly apparent in embryonic tissues, where wound edge cells behave in a strikingly similar manner to DME cells (Wood et al., 2002). Following wounding of the *Drosophila* embryonic epidermis, the cells bordering the wound rapidly polarize their actin cytoskeleton, forming actin protrusions and an actomyosin cable on the edge of the cell facing the wound. As during DC, the actin cable provides a force that drives wound closure and the protrusions assist in fusion of the wound edges (Wood et al., 2002). Epithelial healing in non-embryonic tissues typically occurs by a slightly different mechanism, driven primarily by actin protrusions rather than an actomyosin cable, but is still dependent on polarized actin assembly at the wound edge (Galko and Krasnow, 2004; Martin, 1997).

Assembly of actin at epithelial edges is therefore a conserved process, essential for both epithelial wound healing and DC; however, we have a poor understanding of how this assembly is triggered (Martin and Parkhurst, 2004). A number of reports have suggested that the composition of cell-cell adhesions at the leading edge influences actin assembly during DC (Bahri et al., 2010; Kaltschmidt et al., 2002). For example, recent work has implicated the cell-cell adhesion molecule Echinoid (Laplante and Nilson, 2011). Prior to DC, Echinoid is evenly distributed around the periphery of DME cells, but as DC commences, Echinoid is specifically lost from the leading edge of these cells, and this loss of Echinoid is essential for leading edge actin assembly to occur

[1]The Healing Foundation Centre, Faculty of Life Sciences, University of Manchester, University of Manchester, Michael Smith Building, Oxford Road, Manchester M13 9PT, UK. [2]Department of Physiology, Anatomy and Genetics, University of Oxford, Oxford OX1 3QX, UK.

*These authors contributed equally to this work
‡Author for correspondence (tom.millard@manchester.ac.uk)

Accepted 7 December 2012

(Laplante and Nilson, 2011). The scaffolding protein and apical determinant Par3/Bazooka (Baz) localizes to adherens junctions in the epidermis of DC-stage embryos, but is lost from the leading edge, in concert with Echinoid (Laplante and Nilson, 2011; McKinley et al., 2012). It has been proposed that it is in fact this loss of Baz that triggers actin assembly at the leading edge, although the molecular mechanism linking loss of Baz to assembly of actin at the leading edge is yet to be identified (Laplante and Nilson, 2011).

A good candidate for such a link is phosphoinositide signalling, which is known to regulate polarized actin assembly in other contexts. For example, in *Dictyostelium* and neutrophils, a polarized distribution of the lipid phosphatidylinositol 3,4,5-trisphosphate [PIP3; PtdIns(3,4,5)P_3] within the cell promotes polarized actin assembly, with actin protrusions forming where PIP3 levels are highest (Cain and Ridley, 2009). Polarization of PIP3 within the cell results from spatial variations in the activity of two enzymes: Type I phosphoinositide 3 kinase (PI3K) and Phosphatase and tension homologue (Pten) (Vanhaesebroeck et al., 2012). PI3K catalyses the phosphorylation of phosphatidylinositol 4,5-bisphosphate [PIP2; PtdIns(4,5)P_2] to yield PIP3 while Pten catalyses the reverse reaction, dephosphorylating PIP3 to PIP2. Phosphoinositides are also known to regulate the assembly and apicobasal organization of cell-cell junctions in epithelia, and both PI3K and Pten can associate with cell junction (Kovacs et al., 2002; Shewan et al., 2011; von Stein et al., 2005).

In this study, we use DC and epithelial wound healing in *Drosophila* to explore the mechanism driving actin assembly at epithelial edges. We show that absence of Baz from cell junctions along the epithelial edge is conserved between the leading edge of DC and epithelial wound edges, and we identify a molecular mechanism linking this absence of Baz to the formation of actin protrusions. We find that Pten is recruited to cell-cell junctions by Baz, resulting in low levels of PIP3 at junctions containing Baz. The absence of Baz, and consequently Pten, from cell junctions along the leading edge results in a localized elevation in PIP3 levels, which promotes the formation of actin protrusions. Our findings suggest that Baz couples loss of apicobasal polarity to planar-polarized actin assembly at epithelial edges.

MATERIALS AND METHODS

Fly stocks

w1118 were used as wild-type controls. The following transgenic strains were used: ubiquitous GPH (tGPH) (Britton et al., 2002), ubiquitous GFP-Moesin (cGMA) (Kiehart et al., 2000), UAS-GFP-Moesin (UAS-GMA) (Dutta et al., 2002), UAS-mCherry-Moesin (Millard and Martin, 2008), UAS-Pten3 (Goberdhan et al., 1999), UAS-Pten2 (Huang et al., 1999), UAS-GFP-Pten2, UAS-GFP-Pten3 UAS-PLCγPH-GFP (Pinal et al., 2006), UAS-mCherry-CAAX (Kakihara et al., 2008), UAS-mCherry-Baz (McGill et al., 2009), UAS-CA-Ras1 (Karim and Rubin, 1998), UAS-CA-PI3K (Leevers et al., 1996), UAS-Rac1 (Luo et al., 1994), UAS-E-cadherin-GFP (Oda and Tsukita, 1999), and UAS-Echinoid (Laplante and Nilson, 2011). TubP-Gal4 (Lee and Luo, 1999) was used to express transgenes ubiquitously. *Engrailed*-Gal4 (Brand and Perrimon, 1993) was used to express transgenes in epidermal stripes, e22c-Gal4 (Jacinto et al., 2000) and i76d-Gal4 (derived from DGRC Kyoto stock 106535) were used to express transgenes throughout the epidermis. The following null alleles were used: $baz^{815\text{-}8}$ (Krahn et al., 2010), $PI3K92E^{A}$ (Weinkove et al., 1999) and $Pten^{117}$ (Oldham et al., 2002). Embryos homozygous or hemizygous for these alleles were identified by absence of GFP-expressing balancer chromosomes. Germline clones of $Pten^{117}$ generated using the FLP dominant female sterile technique (Chou and Perrimon, 1996).

UAS-GPH generated by amplifying the GFP-Grp1-PH coding sequence from tGPH flies using primers that introduced a 5′ *Not*I and 3′ *Xba*I site. This construct was cloned into pUASp and transgenic flies generated by BestGene. The G137E mutation was introduced into Pten3 via an overlapping PCR strategy and inserted into pUAST for generation of transgenic flies.

Immunohistochemistry

Immunohistochemistry was performed on flat-filleted embryos (Budnik et al., 2006) fixed with 4% paraformaldehyde. The following antibodies were used: goat anti-GFP (1:500, Abcam); rabbit anti-Baz (1:1000) (von Stein et al., 2005); rat anti-E-cadherin (1:500, DSHB); TRITC- or Alexa647-phalloidin (1:500; Invitrogen); and FITC-, Cy3- or Cy5-conjugated secondary antibodies (donkey, 1:100-200; Jackson ImmunoResearch).

Preparation of *Drosophila* embryos for live imaging

Embryos collected at 25°C on apple juice agar, dechorionated in 50% bleach and mounted in a 3:1 mix of halocarbon oils 700 and 27 (Sigma) between a glass coverslip and a gas-permeable Lumox culture dish (Greiner) as described previously (Evans et al., 2010).

Image acquisition and processing

Images acquired using a Leica TCS-SP5-AOBS confocal microscope (63× NA1.4-HCX-PL-Apo oil objective) or a Nikon A1R confocal microscope (60× NA1.4-CFI-Plan-Apo oil objective). Laser wounding performed using a Micropoint ablation laser (Andor Systems) attached to the Nikon confocal. Images processed and compiled using ImageJ, Volocity, Abode Photoshop and Adobe Illustrator.

Quantitation and data analysis

Measurement of GPH fluorescence along cell junctions performed using ImageJ. All images used for quantitation were acquired using identical microscope settings. To measure zippering rates, embryos were imaged from mid-DC until closure was complete. Relative zippering rates were calculated by measuring the time for the zippering canthus to progress 14 μm either within *en* stripes, or in the intervening non-*en* stripes (i.e. anterior compartments). A mean rate was calculated for *en* stripes and non-*en* stripes for each embryo and then normalized by setting the non-*en* mean as 1. Normalization allowed us to correct for variation in zippering speed between embryos of the same genotype. A mean rate for all embryos in each dataset was calculated using the normalized values and *en* and non-*en* values compared using one-sample *t*-test. Filopodia number/length measured using live mid-DC embryos expressing UAS-GFP-Moesin using *en*-Gal4. Only filopodia exceeding 0.6 μm in length were counted. Datasets compared using Kruskal-Wallis test followed by Dunn's *post hoc* test. Wound areas and protrusion coverage measured using ImageJ. Protrusion coverage datasets compared using the Mann-Whitney test. All data were compiled and graphs prepared using Microsoft Excel; statistical analysis was performed using GraphPad Prism.

RESULTS

Baz is absent from leading edge cell-cell junctions during DC and wound healing

Loss of Baz from the DC leading edge has been postulated to trigger the planar-polarized assembly of F-actin at the leading edge (Laplante and Nilson, 2011). To test whether Baz is also lost from the leading edge during the related process of epithelial wound healing, we compared the distribution of Baz during the two processes. We began by studying the distribution of Baz, E-cadherin and F-actin at the DC leading edge. We found that E-cadherin localized relatively evenly around the periphery of DME cells, except at the F-actin-rich leading edge, where it was slightly enriched at the junctions between neighbouring DME cells that form the attachment points of the leading edge actomyosin cable (Fig. 1Ai). Baz colocalized with E-cadherin around most of the periphery of DME cells, but was absent from actin-rich leading edge, including the junctions between DME cells at which E-cadherin was enriched (Fig. 1A). We also observed this absence of Baz from the leading edge in live embryos expressing fluorescently tagged forms of Baz, E-cadherin and Moesin, a marker of F-actin

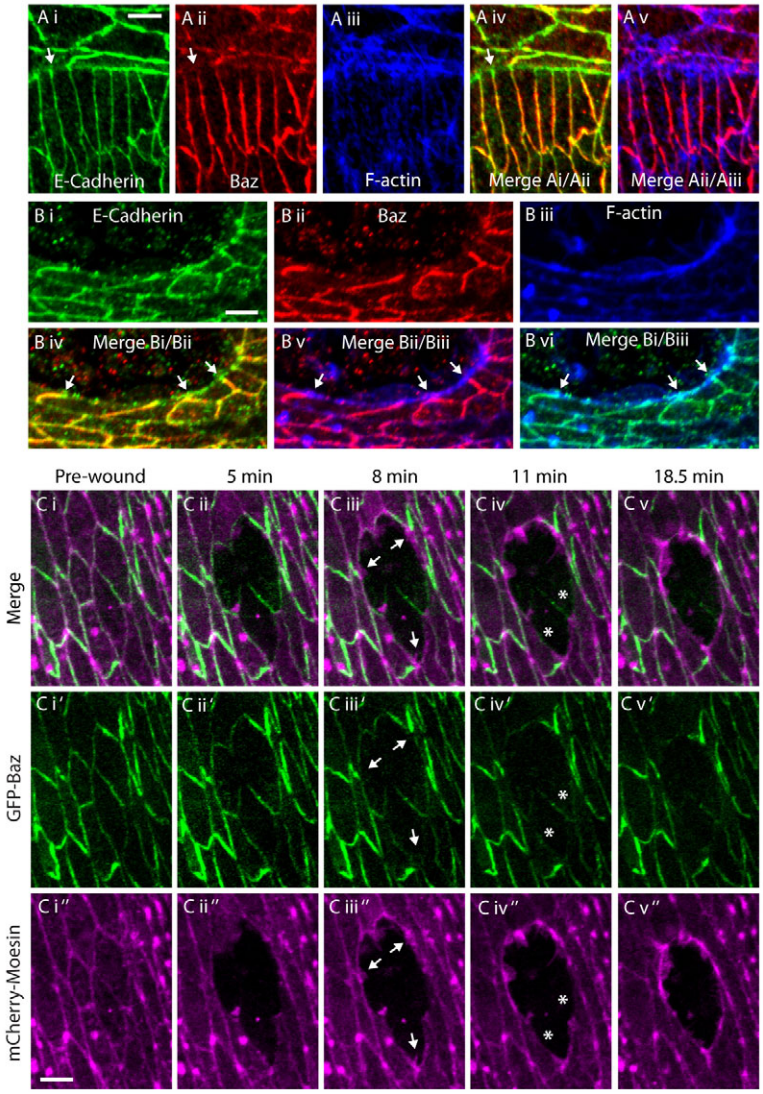

Fig. 1. Baz is absent from cell junctions at the DC leading edge and epithelial wound edges. (**A**) DC leading edge stained for E-cadherin (green), Baz (red) and F-actin (blue) reveals absence of Baz from leading edge. Arrows indicate a leading edge cell-cell junction at which E-cadherin is enriched but Baz is absent. (**B**) Epithelial wound edge stained for E-cadherin (green), Baz (red) and F-actin (blue) reveals Baz is absent from wound edges. Arrows indicate wound edge cell-cell junctions at which E-cadherin and F-actin are present but Baz is absent. (**C**) Time-course of early phase of healing following laser wounding of embryo expressing GFP-Baz (green) and mCherry-Moesin (magenta). Arrows indicate first sites on the wound edge at which Baz is lost and actin accumulates. Later in the process, asterisks indicate sites at which Baz remains at the wound edge and actin accumulation is minimal. Scale bars: 5 μm. Whole sequence shown in supplementary material Movie 1.

(supplementary material Fig. S1). These results therefore confirm that Baz exhibits a planar-polarized distribution in DME cells, reciprocal to that of F-actin.

We next compared the distribution of Baz, E-cadherin and actin at epithelial wound edges. This was carried out by wounding the ventral epidermis of DC-stage embryos with a needle and then fixing embryos 45 minutes later. This revealed that E-cadherin levels were low at the wound edge, except at the junctions between neighbouring wound-edge cells, where E-cadherin was enriched (Fig. 1Bi). Baz was absent from the wound edge, including the wound edge cell-cell junctions at which E-cadherin was enriched (Fig. 1B). Co-staining with phalloidin revealed that the wound edge cell-cell junctions containing E-cadherin, but lacking Baz, corresponded to the attachment points of the actomyosin cable (Fig. 1B). Thus, the reciprocal distribution of Baz and F-actin at the epithelial edge was conserved between DC and wound healing, as was the absence of Baz from cell-cell junctions along the edge. To study the dynamics of Baz loss and F-actin assembly at wound edges, we live imaged wound healing in embryos expressing GFP-Baz and mCherry-Moesin (a marker of F-actin) (Fig. 1C; supplementary material Movie 1). We found that Baz was present along the whole wound edge until around 5 minutes after wounding (Fig. 1Cii). After this, Baz levels at the wound edge began to diminish, and this coincided with the first noticeable accumulations of actin at the wound edge (Fig. 1Ciii). These early actin accumulations occurred at sites at which Baz had been lost and frequently corresponded with junctions between neighbouring wound edge cells (Fig. 1Ciii, arrows). This was followed by a period of around 10 minutes during which there was a gradual increase in actin at the wound edge, which correlated temporally and spatially with a gradual loss of Baz. Throughout this process, regions of the wound edge at which Baz remained exhibited minimal actin assembly (Fig. 1Civ, asterisks). These results revealed that, as during DC, there is a close spatial and temporal correlation between loss of Baz and assembly of F-actin at epithelial wound edges.

Pten is localized to cell-cell junctions by Baz during DC

We next sought to identify potential molecular links between Baz and F-actin assembly that might explain their reciprocal relationship at epithelial edges. For these experiments, we used DC as our model system. A good candidate for such a link is Pten, as it binds directly to Baz and influences actin dynamics by regulating PIP3 levels (Goberdhan et al., 1999; von Stein et al., 2005). We therefore investigated the distribution of Pten during DC. As no effective antibodies were available, we used GFP-tagged Pten to study Pten

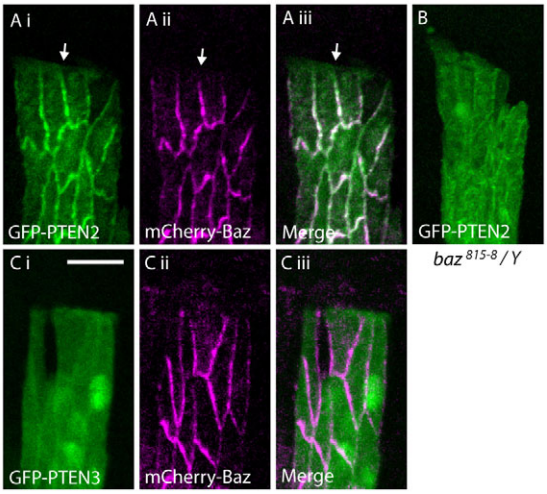

Fig. 2. Pten2 is localized to cell junctions by Baz. (**A**) Expression of UAS-GFP-Pten2 (green) and UAS-mCherry-Baz (magenta) using *en*-Gal4 reveals colocalization of Pten2 and Baz at cell junctions behind the DC leading edge. Arrows indicate leading edge junction at which Baz and Pten2 are absent. (**B**) UAS-GFP-Pten2 (green) expressed using *en*-Gal4 in hemizygous $baz^{815\text{-}8}$ embryo accumulates only weakly at cell junctions. (**C**) Expression of UAS-GFP-Pten3 (green) and UAS-mCherry-Baz (magenta) using *en*-Gal4 reveals that Pten3 exhibits little accumulate at cell junctions. Scale bar: 10 μm.

distribution. The distribution of two Pten splice variants was examined; Pten2 and Pten3, which are identical to one another except that Pten2 possesses a short C-terminal extension that mediates binding to Baz (von Stein et al., 2005). As Pten3 lacks this extension, it is unable to bind to Baz (von Stein et al., 2005). Previous work has suggested that Pten2 is likely to be the predominant splice variant present in DC stage embryos (Maehama et al., 2004). We found that GFP-Pten2 was strongly enriched at cell junctions behind the leading edge, where it co-localized with mCherry-Baz (Fig. 2A). In common with Baz, Pten2 was notably absent from the leading edge, including cell junctions along the leading edge (Fig. 2A, arrows). In contrast to GFP-Pten2, GFP-Pten3, which is unable to bind to Baz (von Stein et al., 2005), exhibited very little accumulation at cell junctions and was instead distributed homogenously throughout the nucleus and cytosol (Fig. 2C). To determine whether the localization of Pten2 to junctions was dependent on Baz, we imaged GFP-Pten2 distribution in embryos lacking zygotic *baz* expression. We found that GFP-Pten2 was largely absent from junctions in hemizygous $baz^{815\text{-}8}$ mutant embryos, instead accumulating more strongly in the cytosol (Fig. 2B). This indicates that the polarized sequestration of Pten2 to cell junctions behind the leading edge is dependent on Baz.

PIP3 accumulates at leading edge cell junctions during DC

In other systems, e.g. *Drosophila* photoreceptor cells and *Dictyostelium*, a polarized distribution of Pten results in polarization of PIP3, with PIP3 accumulating where Pten activity is relatively low (Iijima and Devreotes, 2002; Pinal et al., 2006). This prompted us to examine the distribution of PIP3 at the DC leading edge using the pleckstrin-homology domain of Grp1 fused to GFP (GPH), a well-characterised PIP3 reporter (Britton et al., 2002). As GPH localization was partially lost on embryo fixation, our analyses were largely performed in live embryos. Imaging of live embryos expressing GPH ubiquitously revealed a clear planar-polarization of PIP3 in DME cells, with PIP3 strongly accumulating at their leading edge (Fig. 3Ai). On close inspection, it was apparent that the leading edge accumulation of PIP3 was strongest at the junctions between neighbouring DME cells (Fig. 3Aii). The accumulation of PIP3 at leading edge junctions persisted after zippering, finally being lost around eight cells behind the zippering canthus (Fig. 3Aiii). Behind the leading edge, PIP3 accumulated weakly at cell-cell junctions, more strongly basally than apically (Fig. 3Aiv). No PIP3 could be detected on either the apical or basal surface of epidermal cells. Time-lapse imaging of GPH expressed specifically in stripes of epidermal cells using *engrailed*-Gal4 (*en*-Gal4) allowed a more detailed analysis of PIP3 distribution that eliminated any contribution from the underlying amnioserosa. This confirmed the polarization of PIP3 within DME cells and also showed that PIP3 accumulation at the leading edge was dynamic, changing noticeably over time (Fig. 3B). Co-expression of GPH with a membrane marker (mCherry-CAAX) revealed that the accumulation of PIP3 did not merely reflect elevated quantities of membrane at the leading edge (Fig. 3C). We also observed the distribution of PIP2 during DC using the pleckstrin-homology domain of PLCγ fused to GFP as a reporter, and in contrast to PIP3, PIP2 did not accumulate at leading edge junctions, but was instead homogenously distributed around the periphery of DME cells (Fig. 3D).

The leading edge cell junctions at which PIP3 accumulated appeared to correspond to the junctions at which Baz and Pten were absent. To test this directly, we stained GPH-expressing embryos for Baz. This revealed a clear reciprocal distribution of PIP3 and Baz along the cell junctions of DME cells, with endogenous Baz localizing to cell junctions, except those at the leading edge where PIP3 was enriched (Fig. 3E). This reciprocal distribution can be seen more clearly in live embryos expressing GPH and mCherry-Baz using *en*-Gal4 (Fig. 3F). A sharp transition from PIP3 to Baz is observed at each cell junction just behind the leading edge.

Polarization of PIP3 in DME cells requires Pten and Baz

The reciprocal distribution of PIP3 and Baz/Pten suggested that the accumulation of PIP3 at leading edge junctions might result from the relative absence of Pten activity at these sites. To establish whether the cellular distribution of Pten was responsible for the leading edge PIP3 accumulation, we examined PIP3 distribution in embryos lacking maternal and zygotic Pten expression. As has been described previously, most $Pten^{mat/zyg}$ null embryos die early in embryogenesis; however, a significant number survive until late embryogenesis (von Stein et al., 2005). These embryos exhibited defects in epithelial organization, including irregularly shaped dorsal holes. In DC-stage $Pten^{117mat/zyg}$ embryos, accumulation of GPH at cell junctions throughout the epidermis was markedly greater than in wild-type embryos, indicating that Pten is highly active during DC and plays a major role in suppressing PIP3 levels (Fig. 4A,B). PIP3 was still absent from the apical and basal surfaces of epidermal cells, suggesting either that PIP3 is exclusively generated at cell junctions, or that PIP3 is degraded by an enzyme other than Pten at these locations (Fig. 4B, inset). Notably, the planar-polarized distribution of PIP3 in DME cells was absent in $Pten^{117mat/zyg}$ embryos, with PIP3 now being distributed evenly around the cell periphery (Fig. 4B). Quantitation of GPH fluorescence suggested that this was not because PIP3 levels at leading edge junctions were reduced, but rather that PIP3 levels were elevated at cell-cell junctions behind the leading edge

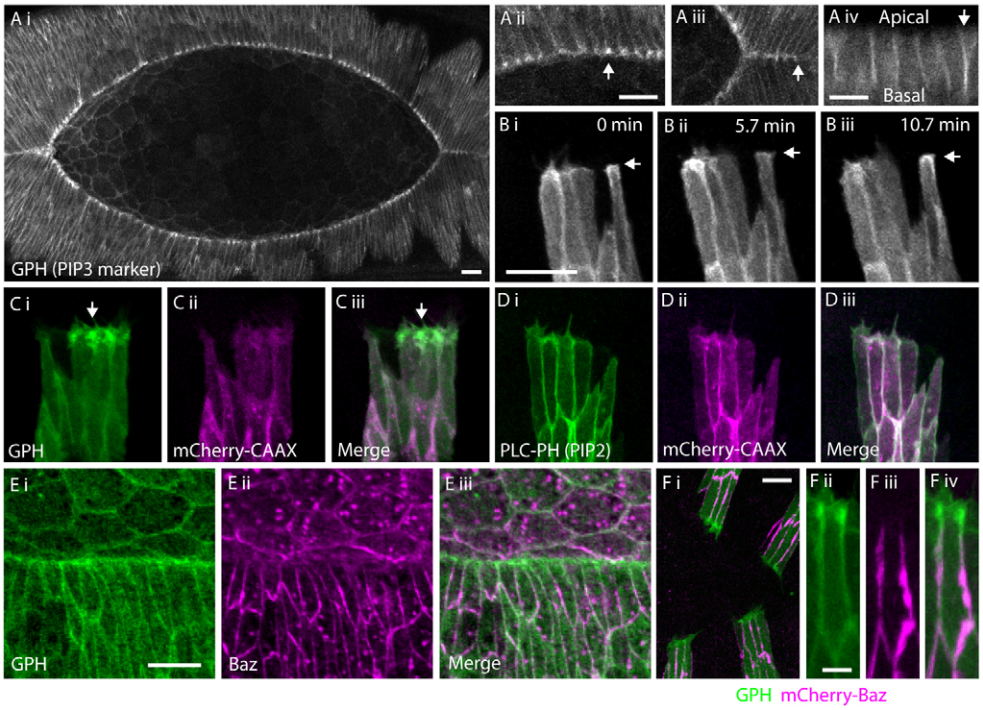

Fig. 3. PIP3 accumulates at the leading edge of DC. (**A**) Ubiquitous expression of GPH reveals accumulation of PIP3 at the DC leading edge, strongest at leading edge cell junctions (arrow, Aii). PIP3 is lost from leading edge approximately eight cells behind zippering canthus (arrow, Aiii). *Z*-section through epidermis (Aiv) reveals PIP3 accumulates specifically at cell-cell junctions, stronger basally than apically (arrow). (**B**) Live imaging of GPH expressed using *en*-Gal4 reveals rapid changes in PIP3 levels at the leading edge (arrows). (**C**,**D**) Co-expression of UAS-GPH (green in C) or UAS-GFP-PLC-PH (green in D) with UAS-mCherry-CAAX (magenta) using *en*-Gal4 reveals that PIP3 accumulates at the leading edge relative to total membrane levels (arrow), whereas PIP2 does not. (**E**) GPH distribution (green) in DME cells is reciprocal to that of endogenous Baz (magenta). (**F**) UAS-GPH (green) and UAS-mCherry-Baz (magenta) expressed using *en*-Gal4 distribute reciprocally in DME cells. Scale bars: 10 μm in Ai-Aiii,B-Eiii,Fi; 5 μm in Aiv; 3 μm in Fii-Fiv.

(Fig. 4C). These data suggest that polarization of Pten distribution along the cell junctions of DME cells does indeed contribute to the polarized accumulation of PIP3 at the leading edge.

As the distribution of Pten along cell junctions of DME cells is determined by that of Baz, we would predict that loss or redistribution of Baz would also perturb the leading edge accumulation of PIP3. We therefore examined the distribution of PIP3 in hemizygous $baz^{815\text{-}8}$ embryos, which lack zygotic expression of *baz*. Our previous experiments showed that in $baz^{815\text{-}8}$ mutant embryos, Pten2 is no longer sequestered to cell junctions behind the leading edge and is instead distributed homogenously throughout the cell (Fig. 2). We found that hemizygous $baz^{815\text{-}8}$ mutant embryos exhibited a significant reduction in PIP3 accumulation at leading edge junctions compared with controls, and a slight increase in PIP3 at junctions behind the leading edge (Fig. 4D-F). This loss of leading edge PIP3 in *baz* mutant embryos is probably caused by a net increase in Pten activity at the leading edge, resulting from the redistribution of Pten2. We next investigated the effect of redistributing Baz within DME cells. This was carried out by expressing exogenous Echinoid in the amnioserosa, which has been shown to prevent Baz from being lost from the leading edge of DC (Laplante and Nilson, 2011). As previously reported, expression of Echinoid in the amnioserosa resulted in a homogenous distribution of Baz around the periphery of DME cells, including the leading edge where it would normally be absent at this stage of DC (Fig. 4G,H). This redistribution of Baz was accompanied by loss of PIP3 accumulation at leading edge cell junctions, supporting the notion that accumulation of PIP3 at the leading edge is dependent on the absence of Baz.

Altering leading edge PIP3 levels affects zippering during DC

We next sought to determine whether PIP3 has a specific function during DC. To do this, we altered leading edge PIP3 levels genetically. To study the effect of reducing PIP3 levels, we used embryos lacking zygotic expression of PI3K92E, the enzyme that synthesizes PIP3. $PI3K92E^{A}$ embryos exhibited a variety of phenotypes, probably resulting from varying maternal contribution, with 11% of embryos failing to reach DC. Of those embryos that reached DC, 19% failed to complete the process, with a further 11% closing but exhibiting puckering at the dorsal seam. One consistent phenotype in $PI3K92E^{A}$ embryos that reached the latter stages of closure was a change in the shape of the dorsal hole (Fig. 5B). Instead of the normal eye-shape, the dorsal hole of $PI3K92E^{A}$ embryos adopted an elongated flattened shape (Fig. 5A,B), such that the length:width ratio of the hole increased to 5.1±0.5 compared with 3.8±0.2 for control embryos ($P<0.005$, $n\geq14$). Using GPH, we confirmed that leading edge PIP3 level were diminished in $PI3K92E^{A}$ embryos (supplementary material Fig. S2A,B). As an alternative method to reduce PIP3 levels, we overexpressed Pten3. This splice variant was chosen as its cytosolic localization made it more effective at reducing leading edge PIP3 than Pten2, which is largely sequestered away from the leading edge by Baz (Fig. 5G). Pten3 expression resulted in an elongation of the dorsal hole, similar to that observed in $PI3K92E^{A}$ mutant embryos [Fig. 5C, length:width ratio 5.2±0.6 compared with 3.6±0.3 for controls ($P<0.001$, $n\geq15$)]. Notably, Baz distribution was not affected by Pten3 overexpression, indicating that Baz distribution determines that of PIP3 and not vice versa (supplementary material Fig. S2C).

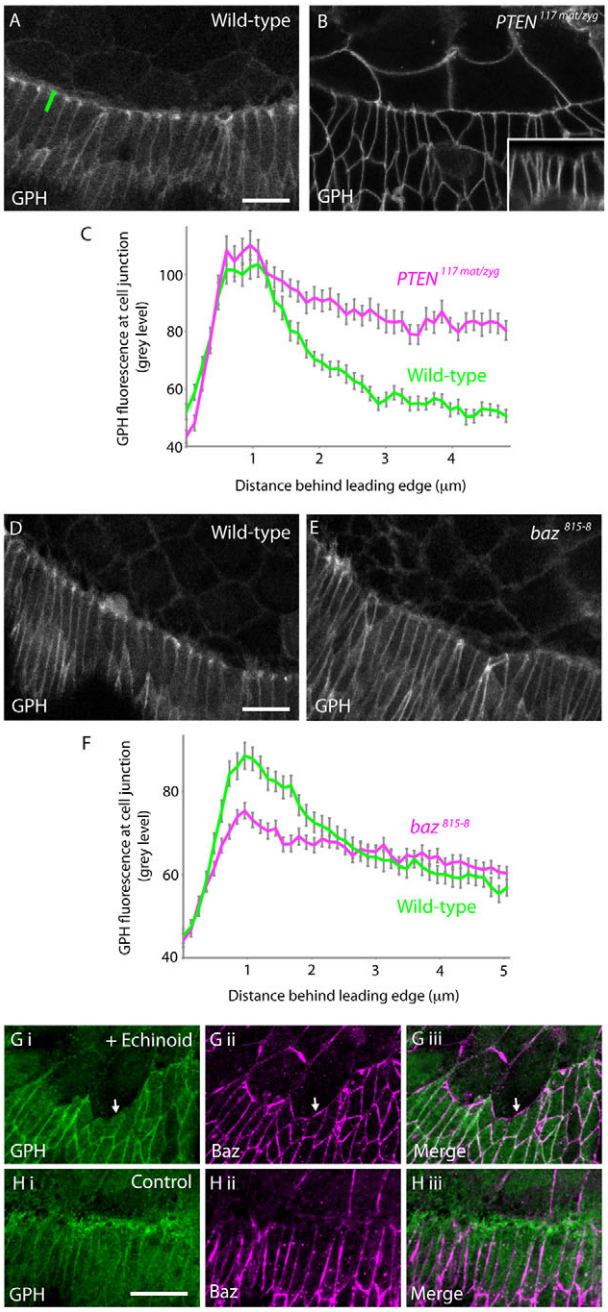

Fig. 4. Pten and Baz are required for polarization of PIP3 in DME cells. (**A**,**B**) Expression of GPH in wild-type (A) or *Pten*$^{117mat/zyg}$ (B) embryos reveals PIP3 distribution is not polarized in DME cells in *Pten*$^{117mat/zyg}$ embryos. Inset in B shows *z*-section through epidermis of *Pten*$^{117mat/zyg}$ embryo (apical is at the top). (**C**) Distribution of PIP3 along junctions between DME cells in wild-type or *Pten*$^{117mat/zyg}$ embryos shows PIP3 levels remain elevated behind the leading edge in *Pten*$^{117mat/zyg}$ embryos. Quantified by measurement of GPH fluorescence intensity along a 5 µm stretch of each junction beginning immediately in front of leading edge, as illustrated by green bar in A. $n \geq 40$ junctions from at least seven embryos. Error bars indicate s.e.m. (**D**,**E**) Expression of GPH in wild-type (D) or hemizygous *baz*$^{815-8}$ (E) embryos shows reduction in leading edge PIP3 accumulation in *baz*$^{815-8}$ embryos. (**F**) Distribution of PIP3 along junctions between DME cells in wild-type or *baz*$^{815-8}$ embryos shows reduced leading edge PIP3 in *baz*$^{815-8}$ embryos. Quantified as described in C. $n \geq 68$ junctions from at least 11 embryos. Error bars indicate s.e.m. (**G**,**H**) Co-staining of GPH (green) and endogenous Baz (magenta) in embryo expressing Echinoid in amnioserosa (G) or in an equivalently staged control embryo (H). Echinoid expression results in the presence of Baz and absence of PIP3 at the leading edge (arrows). Scale bars: 10 µm.

Previous studies have shown that elongation of the dorsal hole can result from a reduction in the speed at which the two epithelial edges zipper together during DC, so we analysed the effect of PIP3 depletion on zippering (Jankovics and Brunner, 2006; Woolner et al., 2005). To do this, we expressed UAS-Pten3 exclusively in the posterior compartment of each segment using *en*-Gal4. This approach had the advantage of limiting depletion of PIP3 to the epidermis and also allowed us to compare zippering of cells with reduced PIP3 levels with that of neighbouring anterior compartment cells in which PIP3 levels were unperturbed. Embryos also expressed GFP-Moesin ubiquitously to allow zippering to be visualized and UAS-mCherry-Moesin to identify UAS-Pten3-expressing cells. Cells overexpressing Pten3 exhibited a significant decrease in zippering speed compared with neighbouring control cells (Fig. 5D,E,L; supplementary material Movies 2, 3). As a result, Pten3-expressing cells frequently zippered later than more central non-expressing cells, leaving transient gaps in the zippering seam (Fig. 5E). Pten is known to have functions that are independent of its ability to dephosphorylate PIP3; notably, it can also dephosphorylate proteins (Myers et al., 1998). To determine whether the effect of overexpressing Pten3 on zippering was due to its protein or lipid phosphatase activity, we analysed zippering in embryos expressing a G137E point mutant of Pten3 (equivalent to G129E in mammalian Pten), which is unable to dephosphorylate PIP3 but retains protein phosphatase activity (Myers et al., 1998; Ramachandran et al., 2009). Expression of Pten3-G137E did not affect zippering speed, indicating that the lipid phosphatase activity of Pten is required for the zippering phenotype (Fig. 5L). To elevate leading edge PIP3 levels, we overexpressed constitutively active PI3K (CA-PI3K) using *en*-Gal4. This had the converse effect to Pten3, increasing zippering speed. As an alternative method to alter leading edge PIP3 levels, we expressed constitutively active Ras1 (CA-Ras), which elevated PIP3 levels, presumably by increasing the activity of endogenous PI3K. In common with CA-PI3K, CA-Ras increased zippering speed (Fig. 5L). These data suggest that leading edge PIP3 regulates zippering during DC.

PIP3 regulates filopodial activity at the DC leading edge

As zippering is dependent on filopodia, we reasoned that the altered zippering speeds observed on modulating PIP3 levels may result from changes in leading edge filopodial activity. We therefore examined leading edge filopodia in embryos in which PIP3 levels were altered using the approaches described in the previous section. The number of filopodia at the leading edge was significantly reduced in zygotic *PI3K92E*^{A} and *baz*$^{815-8}$ mutant embryos, as well as in embryos overexpressing wild-type Pten3; while in embryos expressing the phosphatase-deficient Pten3-G137E, filopodia number was equivalent to controls (Fig. 6A,B). Overexpression of Pten2 appeared to reduce filopodia number slightly, but this did not reach significance in our experiments. The failure of Pten2 to reduce filopodia significantly is probably because much of the Pten2 is sequestered away from the leading edge by Baz. Collectively, these data suggest that the reduced zippering speed observed on depletion of PIP3 is a result of a reduction in filopodia at the leading edge. Consistent with this hypothesis, elevating PIP3 levels by expressing CA-PI3K or CA-Ras resulted in a significant increase in the

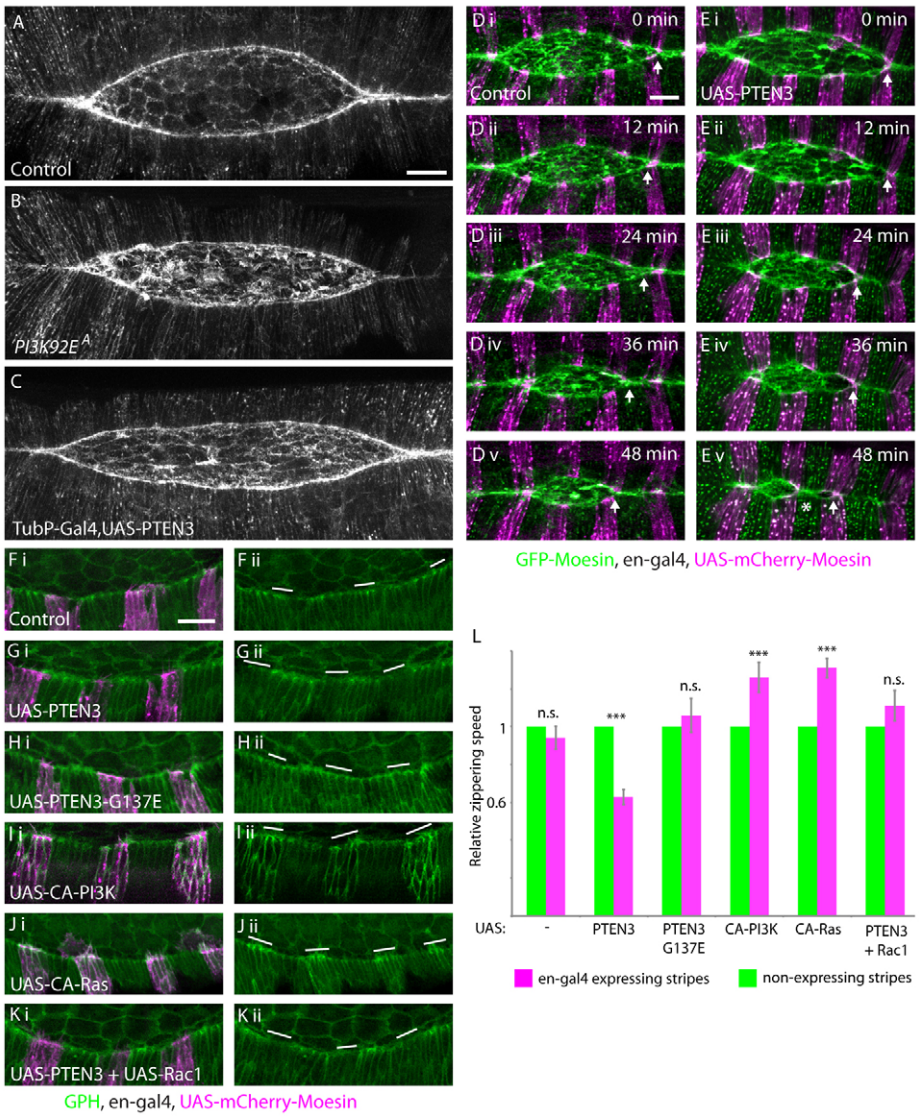

Fig. 5. Modulation of PIP3 levels at the DC leading edge affects zippering. (**A-C**) The dorsal hole is elongated in zygotic *PI3K92E*^{A} embryos (B) and embryos overexpressing UAS-Pten3 ubiquitously using *tubP*-Gal4 (C) compared with controls (A). In each case, embryos express UAS-GFP-Moesin for visualization of dorsal hole. (**D**,**E**) Time-course of latter stages of DC in embryos expressing GFP-Moesin ubiquitously (green) and UAS-mCherry-Moesin (magenta) using *en*-Gal4. Embryo in E also expresses UAS-Pten3 in magenta-labelled cells. Arrows indicate the position of the right-hand zippering canthus in each panel, revealing that zippering proceeds at consistent rate in control embryos, but slows significantly in *en*-Gal4 stripes expressing UAS-Pten3. Asterisk in Ev indicates where slow zippering within Pten3-expressing *en*-Gal4 stripe has resulted in the stripe being 'skipped' by the canthus. (**F-K**) Effect of expression of indicated transgenes on leading edge PIP3 levels revealed by ubiquitous GPH (green). Each transgene is expressed using *en*-Gal4 alongside UAS-mCherry-Moesin (magenta). In Fii-Kii, the mCherry-Moesin channel has been removed; allowing clearer visualization of leading edge PIP3; the location of *en*-Gal4 stripes expressing the transgenes is instead indicated by white bars. Leading edge PIP3 levels are reduced by expression of UAS-Pten3 (G) and UAS-Pten3 + UAS-Rac1 (K), increased by expression of UAS-CA-PI3K (I) and UAS-CA-Ras (J), and unaffected by expression of UAS-Pten3-G137E (H). (**L**) Comparison of zippering speed between *en*-Gal4 stripes (magenta) and intervening non-*en*-Gal4 stripes (green) in embryos expressing the indicated transgenes in *en*-Gal4 stripes. $n \geq 10$ embryos for each transgene. ***$P<0.001$, zippering speed is significantly different between *en*-Gal4 and non-*en*-Gal4 stripes using a one-sample *t*-test; n.s. indicates $P>0.05$. Error bars indicate s.e.m. Scale bars: 15 μm.

filopodia number (Fig. 6A,B). We also observed a correlation between PIP3 levels and filopodia length, although the changes were less pronounced than for filopodia number (supplementary material Fig. S3). We reasoned that if the zippering defect induced by PIP3 depletion was due to reduced filopodial activity, elevating filopodial activity to wild-type levels in PIP3-depleted embryos should rescue the zippering defect. We found that overexpression of the GTPase Rac1 rescued the reduction in filopodial activity induced by Pten without elevating PIP3 levels (Fig. 5K,L; Fig. 6A,B). The increase in filopodia induced by Rac1 was sufficient to rescue the Pten3-induced zippering defect (Fig. 5L). These data strongly suggest that PIP3 promotes zippering during DC by regulating the formation of leading edge filopodia.

To examine the spatial and temporal relationship between PIP3 and filopodia at the leading edge, we live imaged embryos expressing GPH and mCherry-Moesin under the control of *en*-Gal4. This revealed that 61% of filopodia originally arose from a location on the leading edge at which PIP3 was elevated (n=22 embryos).

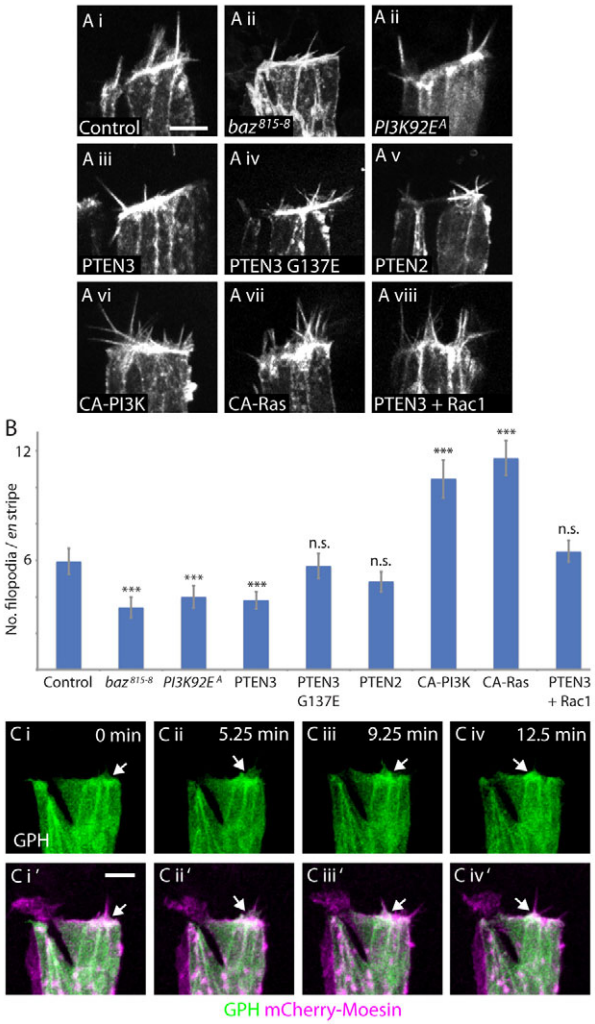

Fig. 6. PIP3 regulates filopodial activity at the DC leading edge. (**A**) Leading edge filopodia imaged in embryos expressing UAS-GFP-Moesin using *en*-Gal4 alongside indicated transgenes or in the indicated mutant. (**B**) Number of filopodia per *en*-Gal4 stripe in embryos expressing indicated transgenes or in indicated mutant. $n \geq 47$ stripes from at least 11 embryos for each genotype. ***$P<0.001$, filopodia number is significantly different from control; n.s. indicates $P>0.05$. Error bars indicate s.e.m. (**C**) Time-course of filopodial dynamics in embryos expressing UAS-mCherry-Moesin (magenta) and UAS-GPH (green) using *en*-Gal4, reveals correlation between PIP3 accumulation and filopodia formation (arrows). Scale bars: 5 µm.

Filopodia usually persisted for longer than the PIP3 accumulations from which they had arisen, suggesting PIP3 may be important for initiation, but not for maintenance, of filopodia. Notably, PIP3 was most concentrated at the base of new filopodia, consistent with a role in initiation (Fig. 6C). The persistence of filopodia after PIP3 had returned to basal levels, and their tendency to exhibit lateral movements away from their point of initiation meant that in most cases still images did not reveal a close spatial correlation between PIP3 and filopodia; however, when filopodial activity was low, a correlation was apparent (Fig. 6C; supplementary material Movie 4).

PIP3 accumulates at epithelial wound edges and promotes actin protrusion formation

As the loss of Baz from cell junctions is conserved between the leading edge of DC and epithelial wound edges, we reasoned the same Pten/PIP3-dependent mechanism might also regulate protrusions at wound edges. We therefore laser wounded embryos expressing GPH and mCherry-Baz throughout the epidermis and live imaged wound healing. As during DC, we observed accumulation of PIP3 along the epithelial leading edge and this accumulation was most pronounced at the junctions between neighbouring wound edge cells (Fig. 7A; supplementary material Movie 5). PIP3 accumulation appeared at one or two wound edge junctions within 10 minutes, then gradually became more widespread, so that eventually PIP3 was enriched at most junctions along the wound edge. As during DC, Baz was largely absent from the cell-cell junctions along the wound edge at which PIP3 was enriched (Fig. 7A). To determine whether PIP3 regulated actin protrusion formation at wound edges, we live imaged wound healing in embryos overexpressing Pten3 in the epidermis alongside mCherry-Moesin. As during DC, overexpression of Pten3 resulted in a significant reduction in actin protrusions at wound edges (Fig. 7B-D). Because actin protrusions contribute to wound closure, this reduction in actin protrusions resulted in a decrease in rate of closure (Fig. 7B,C,E). However, as the formation and contraction of the wound edge actomyosin cable was unaffected by overexpression of Pten3, the reduction in the rate of closure was modest (Fig. 7B,C). These data suggest that regulation of actin protrusions by Baz and PIP3 is conserved between DC and epithelial wound healing.

DISCUSSION

In this paper, we describe a mechanism that drives actin protrusion formation at the edges of epithelial sheets. We find that Baz is specifically lost from cell-cell junctions along the epithelial leading edge during DC and wound healing, and this loss of Baz ultimately leads to protrusion formation by modulating phosphoinositide signalling. This suggests that leading edge junctions play a key role in co-ordinating epithelial migration and closure. The importance of leading edge junctions in regulating actin dynamics during DC has been recognized previously; these junctions are the sites at which the leading edge actomyosin cable and protrusions first form, leading to them to be described as ‘actin nucleation centres’ (Kaltschmidt et al., 2002). It has also been observed that leading edge junctions are rich in actin regulators, including the protrusion-promoting proteins Enabled and Diaphanous, leading to the suggestion that these junctions act as storage sites for proteins required at the leading edge (Homem and Peifer, 2009). We find that bursts of protrusive activity frequently coincide with strong accumulations of PIP3 at leading edge cell junctions, suggesting that PIP3 might trigger the deployment of the protrusion-promoting proteins stored at these sites.

Our data suggest that PIP3 is maintained at low levels throughout most of the epidermis by Pten. This tight control of PIP3 levels is likely to be extremely important as PIP3 regulates a wide variety of cellular processes including growth, proliferation and apicobasal organization (Shewan et al., 2011; Vanhaesebroeck et al., 2012). The absence of Pten from DC and wound leading edges permits PIP3 to become elevated specifically in these locations. It is possible that spatial and temporal variations in PI3K activity also contribute to the elevation of PIP3 at epithelial leading edges. Notably, we observe fluctuations in PIP3 levels at the leading edge that do not appear to be caused by changes in Pten distribution, and so may result from fluctuations in PI3K activity (Fig. 3B; Fig. 6C). We only observe these PIP3 fluctuations at the leading edge, so presumably they are suppressed by Pten elsewhere in the epidermis. PIP3 is known to promote actin assembly in a variety of other systems, the best characterized being chemotaxis of single migrating cells such *Dictyostelium* (Cain and Ridley, 2009). PIP3 also plays a role in

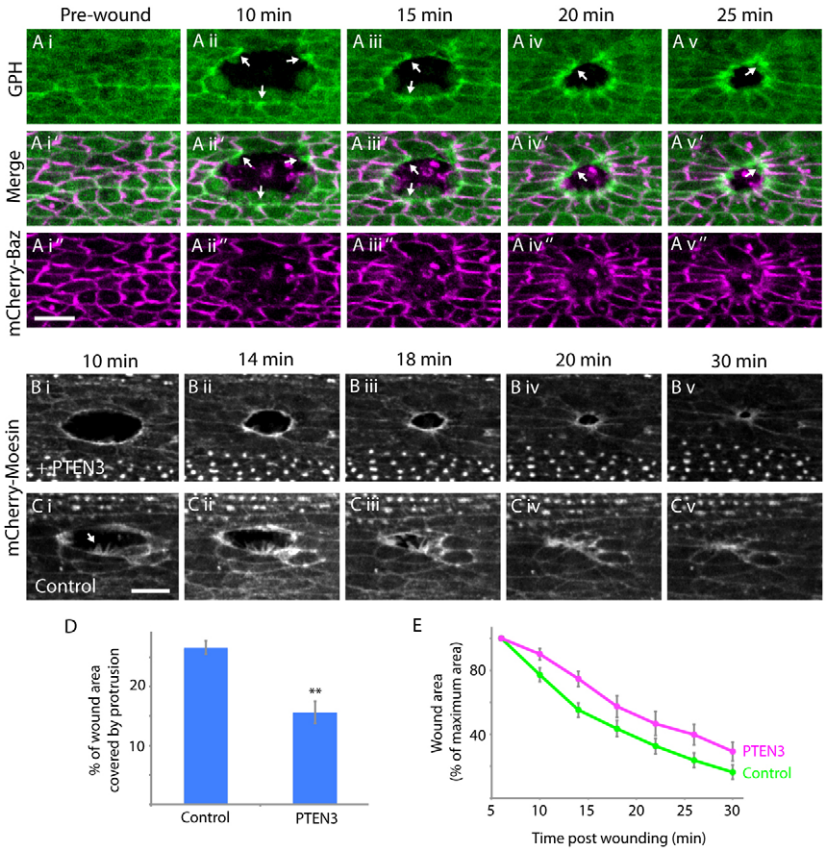

Fig. 7. PIP3 regulates actin protrusion formation at epithelial wound edges. (**A**) Time-course of the early phase of healing following laser wounding of embryo expressing GPH (green) and mCherry-Baz (magenta). Arrows indicate wound edge cell junctions at which GPH is accumulated and Baz is absent. (**B**,**C**) Time-course of wound healing in an embryo overexpressing Pten3 throughout epidermis (B) and in a control embryo (C). Embryos express mCherry-Moesin throughout epidermis for visualization of F-actin. Actin protrusions are widespread along the wound edge in control embryos (arrow in Ci), but rare in Pten-expressing embryos. (**D**) Quantitation of the percentage of wound area covered by protrusions in Pten3-expressing and control embryos. $n \geq 12$ embryos, error bars indicate s.e.m., $^{**}P<0.01$ using the Mann-Whitney test. (**E**) Reduction in wound area over time in Pten3-expressing and control embryos. $n \geq 12$ embryos, error bars indicate s.e.m. Scale bars: 10 μm.

regulating actin assembly in *Drosophila* photoreceptor cells (Pinal et al., 2006). In this process, PIP3 distribution is also regulated by Baz and Pten, although in this instance PIP3 is polarized apicobasally.

We currently do not know the molecular mechanism by which PIP3 promotes protrusion formation at epithelial edges. In other systems, PIP3 promotes actin protrusion formation by activating the small GTPase Rac and notably PIP3 depletion produces a similar DC phenotype to loss of Rac, suggesting Rac might act downstream of PIP3 during DC (Cain and Ridley, 2009; Woolner et al., 2005). Rac promotes actin protrusion formation in the *Drosophila* pupal notum and, interestingly, these protrusions are restricted to regions of the cell devoid of Baz, suggesting an analogous signalling process may be operating (Georgiou and Baum, 2010).

Previous work has shown that if Baz is retained at the leading edge during DC, the formation of both the contractile actomyosin cable and actin protrusions are inhibited (Laplante and Nilson, 2011). As depletion of PIP3 did not block actomyosin cable assembly, loss of Baz must also trigger a PIP3-independent pathway that drives cable assembly. Baz exhibits a reciprocal distribution to actomyosin in other processes in the *Drosophila* embryo, including germband extension and amnioserosa remodelling; however, the molecular basis of this reciprocal relationship is not well understood, although recent work has indicated that Rho-kinase is involved (Pope and Harris, 2008; Simões et al., 2010; Zallen and Wieschaus, 2004).

Cell-cell junctions are clearly well placed to detect a loss of epithelial integrity and transduce a signal to activate the motility machinery of a cell in response. Our data suggest that loss of Baz from junctions at the epithelial leading edge is an early event in this signal transduction process. An important unanswered question is what triggers Baz to be lost from leading edge junctions. One possibility is that cell-cell junctions can sense changes in their mechanical environment that result from loss of epithelial integrity, and respond by changing their structure and composition. Previous work has shown that other components of apicobasally polarized cell-cell junctions are also lost from the DC leading edge, suggesting that absence of Baz reflects a general breakdown of apicobasal polarity at epithelial edges (Bahri et al., 2010). The leading edge therefore undergoes a transition from an apicobasally polarized non-motile state to a planar-polarized motile state as DC commences. Our data suggests that Baz plays a key role in coordinating this transition. Disassembly of F-actin at the leading edge after completion of DC coincides with the reappearance of Baz, suggesting Baz may also direct the transition back to a non-motile state when epithelial integrity has been re-established (Laplante and Nilson, 2011).

In summary, this paper reveals a novel mechanism that triggers actin protrusion formation at epithelial edges in response to changes in the composition of cell-cell adhesions. This highlights the importance of cell-cell adhesions as sensors of epithelial integrity and activators of epithelial repair mechanisms. It will be interesting to determine how widely the mechanisms described in this paper are conserved in other organisms and tissues, and in particular whether they are conserved in tissues exhibiting different modes of epithelial repair.

Acknowledgements
We thank Andreas Wodarz, Clive Wilson, Andreas Prokop, Laura Nilson, Tony Harris and Brian Stramer for providing fly stocks and antibodies. We are grateful to Sarah Woolner, Enrique Amaya and Chris Thompson for critically reading this manuscript, and to the Faculty of Life Sciences and Bioimaging and Fly facilities for technical assistance.

Funding
This research was funded by the Healing Foundation, the Dowager Eleanor Peel Trust and the Biotechnology and Biological Sciences Research Council [BB/I007288/1].

Competing interests statement
The authors declare no competing financial interests.

Supplementary material
Supplementary material available online at
http://dev.biologists.org/lookup/suppl/doi:10.1242/dev.089557/-/DC1

References

Bahri, S., Wang, S., Conder, R., Choy, J., Vlachos, S., Dong, K., Merino, C., Sigrist, S., Molnar, C., Yang, X. et al. (2010). The leading edge during dorsal closure as a model for epithelial plasticity: Pak is required for recruitment of the Scribble complex and septate junction formation. *Development* **137**, 2023-2032.
Brand, A. H. and Perrimon, N. (1993). Targeted gene expression as a means of altering cell fates and generating dominant phenotypes. *Development* **118**, 401-415.
Britton, J. S., Lockwood, W. K., Li, L., Cohen, S. M. and Edgar, B. A. (2002). Drosophila's insulin/PI3-kinase pathway coordinates cellular metabolism with nutritional conditions. *Dev. Cell* **2**, 239-249.
Budnik, V., Gorczyca, M. and Prokop, A. (2006). Selected methods for the anatomical study of Drosophila embryonic and larval neuromuscular junctions. *Int. Rev. Neurobiol.* **75**, 323-365.
Cain, R. J. and Ridley, A. J. (2009). Phosphoinositide 3-kinases in cell migration. *Biol. Cell* **101**, 13-29.
Chou, T. B. and Perrimon, N. (1996). The autosomal FLP-DFS technique for generating germline mosaics in Drosophila melanogaster. *Genetics* **144**, 1673-1679.
Dutta, D., Bloor, J. W., Ruiz-Gomez, M., VijayRaghavan, K. and Kiehart, D. P. (2002). Real-time imaging of morphogenetic movements in Drosophila using Gal4-UAS-driven expression of GFP fused to the actin-binding domain of moesin. *Genesis* **34**, 146-151.
Evans, I. R., Zanet, J., Wood, W. and Stramer, B. M. (2010). Live imaging of Drosophila melanogaster embryonic hemocyte migrations. *J. Vis. Exp.* **36**, 1696.
Galko, M. J. and Krasnow, M. A. (2004). Cellular and genetic analysis of wound healing in Drosophila larvae. *PLoS Biol.* **2**, E239.
Garcia-Fernandez, B., Campos, I., Geiger, J., Santos, A. C. and Jacinto, A. (2009). Epithelial resealing. *Int. J. Dev. Biol.* **53**, 1549-1556.
Georgiou, M. and Baum, B. (2010). Polarity proteins and Rho GTPases cooperate to spatially organise epithelial actin-based protrusions. *J. Cell Sci.* **123**, 1089-1098.
Goberdhan, D. C., Paricio, N., Goodman, E. C., Mlodzik, M. and Wilson, C. (1999). Drosophila tumor suppressor PTEN controls cell size and number by antagonizing the Chico/PI3-kinase signaling pathway. *Genes Dev.* **13**, 3244-3258.
Harden, N. (2002). Signaling pathways directing the movement and fusion of epithelial sheets: lessons from dorsal closure in Drosophila. *Differentiation* **70**, 181-203.
Homem, C. C. and Peifer, M. (2009). Exploring the roles of diaphanous and enabled activity in shaping the balance between filopodia and lamellipodia. *Mol. Biol. Cell* **20**, 5138-5155.
Huang, H., Potter, C. J., Tao, W., Li, D. M., Brogiolo, W., Hafen, E., Sun, H. and Xu, T. (1999). PTEN affects cell size, cell proliferation and apoptosis during Drosophila eye development. *Development* **126**, 5365-5372.
Iijima, M. and Devreotes, P. (2002). Tumor suppressor PTEN mediates sensing of chemoattractant gradients. *Cell* **109**, 599-610.
Jacinto, A., Wood, W., Balayo, T., Turmaine, M., Martinez-Arias, A. and Martin, P. (2000). Dynamic actin-based epithelial adhesion and cell matching during Drosophila dorsal closure. *Curr. Biol.* **10**, 1420-1426.
Jankovics, F. and Brunner, D. (2006). Transiently reorganized microtubules are essential for zippering during dorsal closure in Drosophila melanogaster. *Dev. Cell* **11**, 375-385.
Kakihara, K., Shinmyozu, K., Kato, K., Wada, H. and Hayashi, S. (2008). Conversion of plasma membrane topology during epithelial tube connection requires Arf-like 3 small GTPase in Drosophila. *Mech. Dev.* **125**, 325-336.
Kaltschmidt, J. A., Lawrence, N., Morel, V., Balayo, T., Fernández, B. G., Pelissier, A., Jacinto, A. and Martinez Arias, A. (2002). Planar polarity and actin dynamics in the epidermis of Drosophila. *Nat. Cell Biol.* **4**, 937-944.
Karim, F. D. and Rubin, G. M. (1998). Ectopic expression of activated Ras1 induces hyperplastic growth and increased cell death in Drosophila imaginal tissues. *Development* **125**, 1-9.
Kiehart, D. P., Galbraith, C. G., Edwards, K. A., Rickoll, W. L. and Montague, R. A. (2000). Multiple forces contribute to cell sheet morphogenesis for dorsal closure in Drosophila. *J. Cell Biol.* **149**, 471-490.
Kovacs, E. M., Ali, R. G., McCormack, A. J. and Yap, A. S. (2002). E-cadherin homophilic ligation directly signals through Rac and phosphatidylinositol 3-kinase to regulate adhesive contacts. *J. Biol. Chem.* **277**, 6708-6718.
Krahn, M. P., Klopfenstein, D. R., Fischer, N. and Wodarz, A. (2010). Membrane targeting of Bazooka/PAR-3 is mediated by direct binding to phosphoinositide lipids. *Curr. Biol.* **20**, 636-642.
Laplante, C. and Nilson, L. A. (2011). Asymmetric distribution of Echinoid defines the epidermal leading edge during Drosophila dorsal closure. *J. Cell Biol.* **192**, 335-348.
Lee, T. and Luo, L. (1999). Mosaic analysis with a repressible cell marker for studies of gene function in neuronal morphogenesis. *Neuron* **22**, 451-461.
Leevers, S. J., Weinkove, D., MacDougall, L. K., Hafen, E. and Waterfield, M. D. (1996). The Drosophila phosphoinositide 3-kinase Dp110 promotes cell growth. *EMBO J.* **15**, 6584-6594.
Luo, L., Liao, Y. J., Jan, L. Y. and Jan, Y. N. (1994). Distinct morphogenetic functions of similar small GTPases: Drosophila Drac1 is involved in axonal outgrowth and myoblast fusion. *Genes Dev.* **8**, 1787-1802.
Maehama, T., Kosaka, N., Okahara, F., Takeuchi, K., Umeda, M., Dixon, J. E. and Kanaho, Y. (2004). Suppression of a phosphatidylinositol 3-kinase signal by a specific spliced variant of Drosophila PTEN. *FEBS Lett.* **565**, 43-47.
Martin, P. (1997). Wound healing – aiming for perfect skin regeneration. *Science* **276**, 75-81.
Martin, P. and Parkhurst, S. M. (2004). Parallels between tissue repair and embryo morphogenesis. *Development* **131**, 3021-3034.
McGill, M. A., McKinley, R. F. and Harris, T. J. (2009). Independent cadherin-catenin and Bazooka clusters interact to assemble adherens junctions. *J. Cell Biol.* **185**, 787-796.
McKinley, R. F., Yu, C. G. and Harris, T. J. (2012). Assembly of Bazooka polarity landmarks through a multifaceted membrane-association mechanism. *J. Cell Sci.* **125**, 1177-1190.
Millard, T. H. and Martin, P. (2008). Dynamic analysis of filopodial interactions during the zippering phase of Drosophila dorsal closure. *Development* **135**, 621-626.
Myers, M. P., Pass, I., Batty, I. H., Van der Kaay, J., Stolarov, J. P., Hemmings, B. A., Wigler, M. H., Downes, C. P. and Tonks, N. K. (1998). The lipid phosphatase activity of PTEN is critical for its tumor supressor function. *Proc. Natl. Acad. Sci. USA* **95**, 13513-13518.
Oda, H. and Tsukita, S. (1999). Nonchordate classic cadherins have a structurally and functionally unique domain that is absent from chordate classic cadherins. *Dev. Biol.* **216**, 406-422.
Oldham, S., Stocker, H., Laffargue, M., Wittwer, F., Wymann, M. and Hafen, E. (2002). The Drosophila insulin/IGF receptor controls growth and size by modulating PtdInsP(3) levels. *Development* **129**, 4103-4109.
Pinal, N., Goberdhan, D. C., Collinson, L., Fujita, Y., Cox, I. M., Wilson, C. and Pichaud, F. (2006). Regulated and polarized PtdIns(3,4,5)P3 accumulation is essential for apical membrane morphogenesis in photoreceptor epithelial cells. *Curr. Biol.* **16**, 140-149.
Pope, K. L. and Harris, T. J. (2008). Control of cell flattening and junctional remodeling during squamous epithelial morphogenesis in Drosophila. *Development* **135**, 2227-2238.
Ramachandran, P., Barria, R., Ashley, J. and Budnik, V. (2009). A critical step for postsynaptic F-actin organization: regulation of Baz/Par-3 localization by aPKC and PTEN. *Dev. Neurobiol.* **69**, 583-602.
Shewan, A., Eastburn, D. J. and Mostov, K. (2011). Phosphoinositides in cell architecture. *Cold Spring Harb. Perspect. Biol.* **3**, a004796.
Simões, S. M., Blankenship, J. T., Weitz, O., Farrell, D. L., Tamada, M., Fernandez-Gonzalez, R. and Zallen, J. A. (2010). Rho-kinase directs Bazooka/Par-3 planar polarity during Drosophila axis elongation. *Dev. Cell* **19**, 377-388.
Vanhaesebroeck, B., Stephens, L. and Hawkins, P. (2012). PI3K signalling: the path to discovery and understanding. *Nat. Rev. Mol. Cell Biol.* **13**, 195-203.
von Stein, W., Ramrath, A., Grimm, A., Müller-Borg, M. and Wodarz, A. (2005). Direct association of Bazooka/PAR-3 with the lipid phosphatase PTEN reveals a link between the PAR/aPKC complex and phosphoinositide signaling. *Development* **132**, 1675-1686.
Weinkove, D., Neufeld, T. P., Twardzik, T., Waterfield, M. D. and Leevers, S. J. (1999). Regulation of imaginal disc cell size, cell number and organ size by Drosophila class I(A) phosphoinositide 3-kinase and its adaptor. *Curr. Biol.* **9**, 1019-1029.
Wood, W., Jacinto, A., Grose, R., Woolner, S., Gale, J., Wilson, C. and Martin, P. (2002). Wound healing recapitulates morphogenesis in Drosophila embryos. *Nat. Cell Biol.* **4**, 907-912.
Woolner, S., Jacinto, A. and Martin, P. (2005). The small GTPase Rac plays multiple roles in epithelial sheet fusion – dynamic studies of Drosophila dorsal closure. *Dev. Biol.* **282**, 163-173.
Zallen, J. A. and Wieschaus, E. (2004). Patterned gene expression directs bipolar planar polarity in Drosophila. *Dev. Cell* **6**, 343-355.

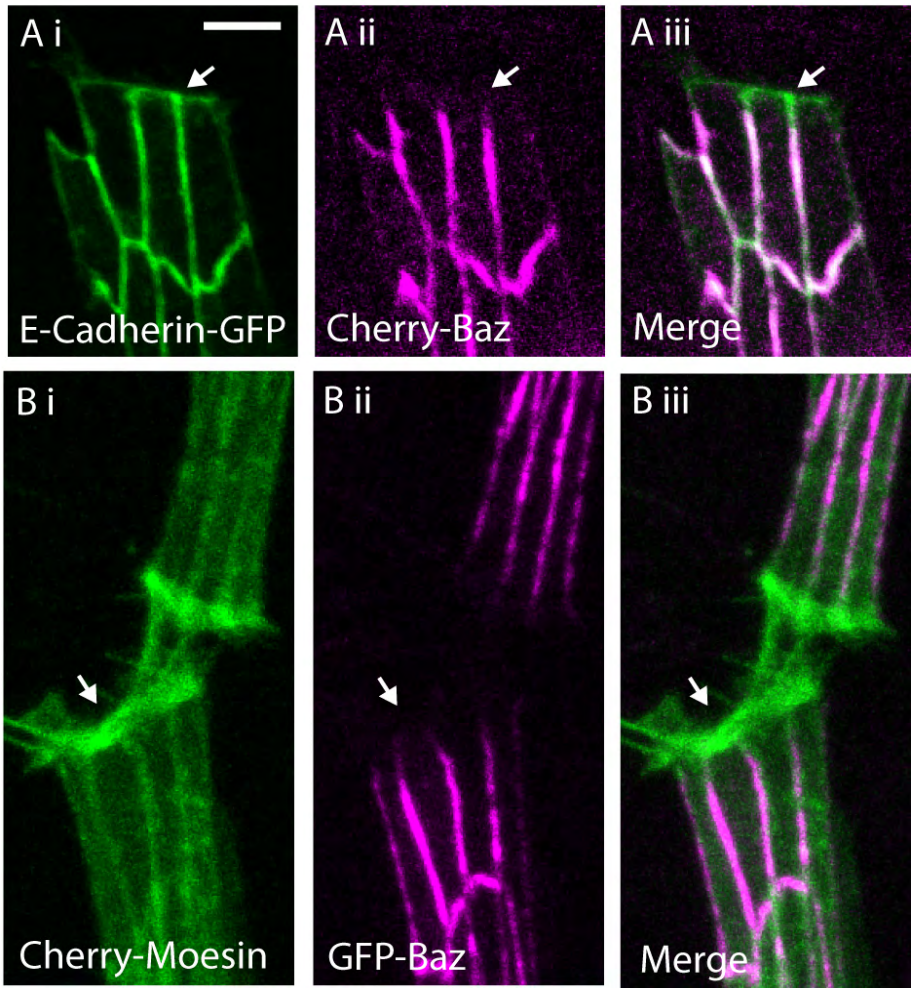

Fig. S1. Baz is absent from the leading edge in live embryos. (**A**) UAS-E-cadherin-GFP (green) and UAS-mCherry-Baz (magenta) expressed using *en*-Gal4 reveals absence of Baz from leading edge cell-cell junctions (arrows). (**B**) UAS-mCherry-Moesin (green) and UAS-GFP-Baz (magenta) expressed using *en*-Gal4 reveals absence of Baz from actin-rich region of the leading edge (arrows). Scale bar: 5 µm.

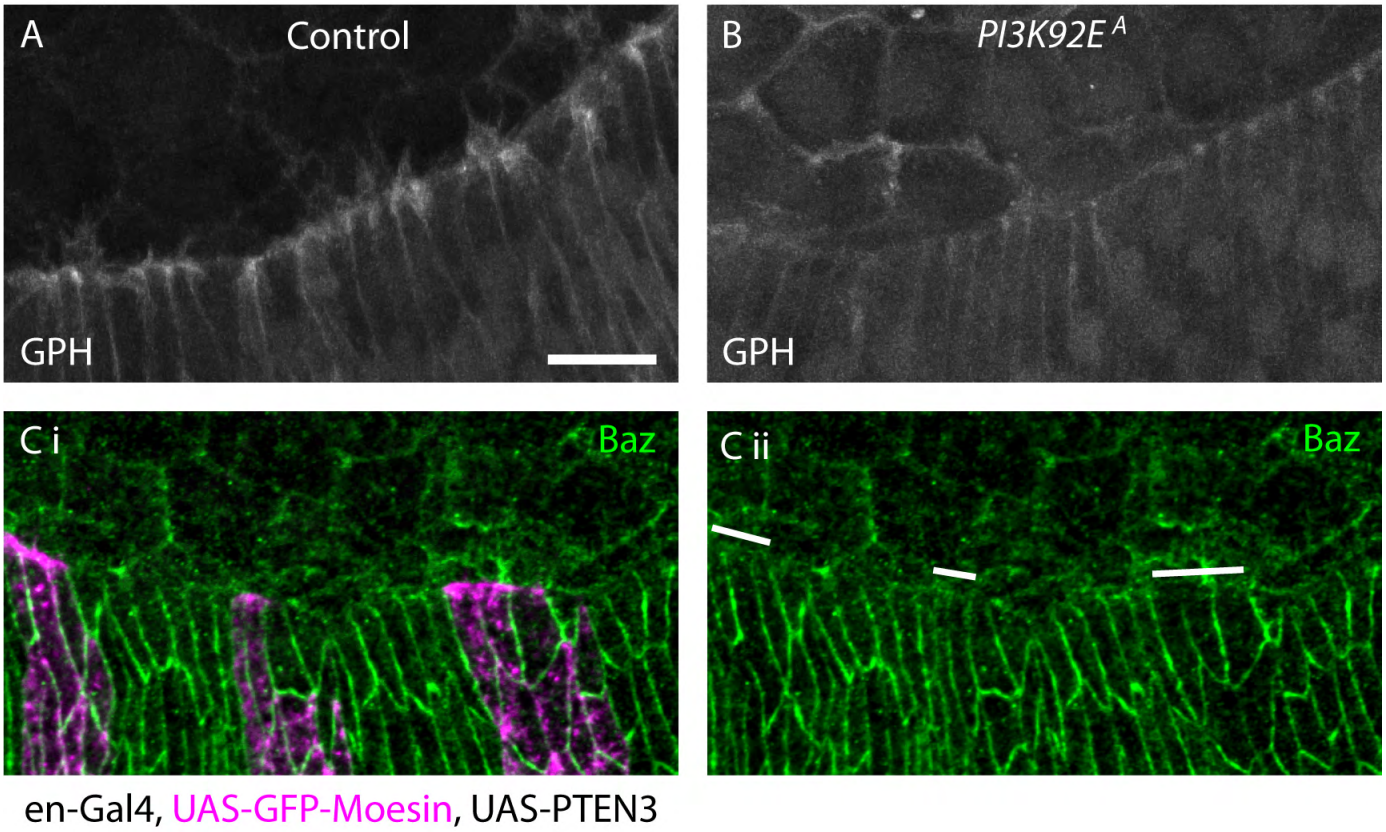

Fig. S2. PIP3 distribution in zygotic *PI3K92E* mutant embryo and Baz distribution in Pten3-expressing embryo. (**A**,**B**) GPH expressed ubiquitously in wild-type (A) or *PI3K92E*^{A} zygotic mutant (B) embryos reveals that leading edge PIP3 is severely depleted in the absence of zygotic PI3K expression. (**C**) Staining of endogenous Baz (green) in an embryo expressing UAS-Pten3 in stripes using *en*-Gal4 reveals that cellular distribution of Baz is unaffected by depletion of PIP3. UAS-GFP-Moesin (magenta) is also expressed under control of *en*-Gal4 to allow Pten3-expressing cells to be identified. Magenta channel has been removed from Cii and Pten3-expressing cells are instead indicated by white bars. Scale bar: 10 µm.

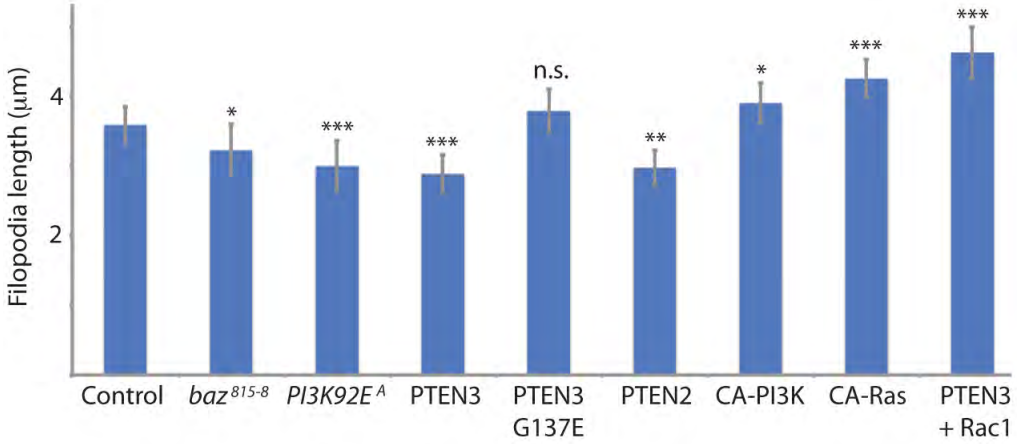

Fig. S3. Effect of altering PIP3 on filopodia length. Length of leading edge filopodia measured in embryos expressing UAS-GFP-Moesin using *en*-Gal4 alongside the indicated transgenes or in indicated mutant. $n \geq 47$ stripes from at least 11 embryos for each genotype. ***$P<0.001$, filopodia length significantly different from control. **$P<0.01$, *$P<0.05$, n.s. indicates $P>0.05$. Error bars indicate s.e.m.

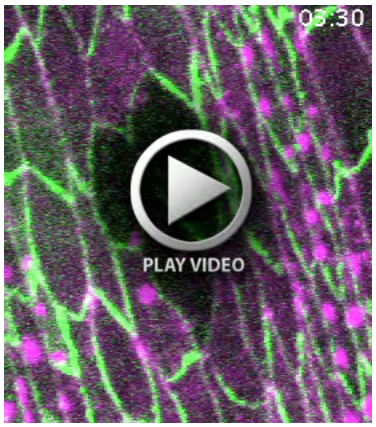

Movie 1. Dynamics of actin and Baz during epithelial wound healing. Live imaging of laser wound healing in an embryo expressing GFP-Baz (green) and mCherry-Moesin (magenta) reveals that accumulation of actin at the wound edge coincides with the loss of Baz. Images are recorded at 90-second intervals. Stills are shown in Fig. 1C.

Movie 2. Zippering during DC occurs at a consistent rate in a control embryo. Live imaging of the last stage of DC in an embryo expressing GFP-Moesin ubiquitously (green) and UAS-mCherry-Moesin (magenta) using *en*-Gal4 shows that zippering proceeds at a similar rate in *en*-Gal4-expressing stripes and in the intervening non-*en*-Gal4 stripes. Images are recorded at 120-second intervals. Stills are shown in Fig. 5D.

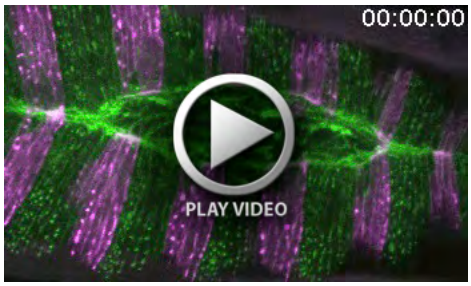

Movie 3. Zippering speed is reduced in cells overexpressing PTEN3. Live imaging of the last stage of DC in an embryo expressing GFP-Moesin ubiquitously (green) with UAS-mCherry-Moesin (magenta) and UAS-Pten3 expressed using *en*-Gal4. Zippering is slower in the *en*-Gal4 stripes expressing Pten3, such that stripes are skipped by the zippering canthus. Images are recorded at 120-second intervals. Stills are shown in Fig. 5E.

Movie 4. Filopodia form at locations on the leading edge at which PIP3 levels are elevated. Live imaging of DC in an embryo expressing UAS-GPH (green) and UAS-mCherry-Moesin (magenta) using *en*-Gal4 reveals spatial and temporal correlation between accumulation of PIP3 at the leading edge and initiation of filopodia. Images are recorded at 15-second intervals. Stills are shown in Fig. 6C.

Movie 5. PIP3 accumulates at cell-cell junctions along epithelial wound edges. Live imaging of laser wound healing in embryo expressing GPH (green) and mCherry-Baz (magenta) in the epidermis reveals that PIP3 accumulates at wound edge cell-cell junctions. Junctions at which PIP3 accumulates are devoid of Baz. Images are recorded at 150-second intervals. Stills shown in Fig. 7A.